Digital Object Identifier

A Bluetooth 5.1 Dataset Based on Angle of Arrival and RSS for Indoor Localization

Michele Girolami [1], Francesco Furfari [1], Paolo Barsocchi [1] and Fabio Mavilia [1]
[1]Italian National Council of Research, ISTI-CNR, Pisa, Italy (e-mail: name.surname@isti.cnr.it)

Corresponding author: Michele Girolami(e-mail: michele.girolami@isti.cnr.it).

This work is partially supported by the ChAALenge project CUP: B89J22002310005 and co-funded by European Union - Next Generation EU, in the context of The National Recovery and Resilience Plan, Investment Partenariato Esteso PE8 "Conseguenze e sfide dell'invecchiamento", Project Age-IT, CUP: B83C22004800006.

ABSTRACT Several Radio-Frequency technologies have been explored to evaluate the efficacy of localization algorithms in indoor environments, including Received Signal Strength (RSS), Time of Flight (ToF), and Angle of Arrival (AoA). Among these, AoA technique has been gaining interest when adopted with the Bluetooth protocol. In this work, we describe a data collection measurement campaign of AoA and RSS values collected from Bluetooth 5.1 compliant tags and a set of anchor nodes deployed in the environment. We detail the adopted methodology to collect the dataset and we report all the technical details to reproduce the data collection process. The resulting dataset and the adopted software is publicly available to the community. To collect the dataset, we deploy four anchor nodes and four Bluetooth tags and we reproduce some representative scenarios for indoor localization: calibration, static, mobility, and proximity. Each scenario is annotated with an accurate ground truth (GT). We also assess the quality of the collected data. Specifically, we compute the Mean Absolute Error (MAE) between the AoA estimated by the anchors and the corresponding GT. Additionally, we investigate the packet loss metric which measures the percentage of Bluetooth beacons lost by the anchors.

INDEX TERMS Angle of Arrival, Bluetooth, Indoor Localization, Dataset

I. INTRODUCTION

THE effectiveness of an indoor localization system greatly depends on the adopted technologies exploited to estimate the position of a target. In the last 10 years, many technologies have been adopted to this purpose, ranging from light and acoustic signals to RF-based (Radio Frequency) approaches [1], [2]. In particular, the family of RF techniques represents one of the most investigated research fields for a couple of reasons. On the one hand, some wireless signals, i.e., UWB (Ultra Wide Band modulating up to 10 GHz and based on Time of Arrival [3]), can penetrate indoor obstacles, such as furniture or walls, hence reducing the impact of human bodies on signal propagation [4]. On the other hand, an increasing number of wireless interfaces are already available with commercial products [5], thus enabling the possibility of localizing a person while moving indoor. Among the RF technologies, we refer to Bluetooth and, in particular, to the 5.1 Direction Finding (DF) specification, according to which a device equipped with an antenna array can estimate the angle on reception of messages from an emitter. In particular, the DF specification considers the Angle of Arrival (AoA) and the Angle of Departure (AoD) [6]–[8].

To the best of our knowledge, evaluating AoA-based localization techniques with the existing datasets is difficult. Indeed, only few datasets provide AoA values in representative environments, suitable for indoor localization. In addition, the lack of details concerning the experimental settings makes difficult to reproduce the results.

This *Methods* paper describes an extensive data collection campaign specifically designed for indoor localization and based on Bluetooth 5.1 commercial devices. We describe the adopted methodology for the data collection and all the technical details required to reproduce the experiments reported in this work.

In particular, the novelties of this work can be summarized as follows:

- A public dataset with data obtained from four representative scenarios. The dataset includes accurate ground

truth (GT), Angle of Arrival and RSS values from commercial Bluetooth 5.1 devices. The dataset allows reproducing indoor localization and proximity detection algorithms at realistic conditions;
- The study of how AoA and RSS vary at specific conditions, so that to assess the potentialities of AoA for the design of indoor localization algorithms.

The resulting dataset is available online to the community [9] and, to the best of our knowledge, it is the first public datasets collecting AoA and RSS values for indoor localization. Moreover, we release to the community also the adopted software to collect the GT.

Data are collected in a wide open room of approximately 110 m^2 and equipped with four anchor nodes deployed on the room's perimeter. We also employed several Bluetooth tags broadcasting beacons at periodic intervals. Anchor nodes log the following information: the timestamp, the AoA value on the azimuth and elevation planes, the RSS of two polarizations expressed in decibel and the Bluetooth channel on which every beacon message is received (three Bluetooth channels are used). The tested scenarios include a calibration phase, in which we collect data from a tag mounted on a tripod resting in 119 different locations. This first scenario allows studying how AoA varies in the environment, limiting the noisy effect of human's bodies. The second scenario is obtained with a person holding a tag around her neck and resting in 36 different locations. Not only, but we reproduce this scenario by varying the relative orientation of the person: North, East, West and South orientations. This scenario enables the study of AoA is altered by the human body. The third scenario considers three mobility use-cases, each reproducing a person moving along a path and holding the tag around the neck. During these tests, the person acts with a *natural* behaviour and moves with a typical pedestrian step length and speed. Lastly, we implement a proximity scenario. With the term proximity, we refer to a situation in which a person gets close to another person or to a Point of Interest (POI). We reproduce 4 proximity use-cases: proximity of a person with 5 POIs, proximity of a group of 4 people, proximity of a triad and proximity of 2 couples. All scenarios include an accurate GT annotation, detailing the actual location of the tag and the corresponding timestamp.

This work also includes a preliminary analysis of the dataset. More specifically, we compute the Mean Absolute Error (MAE) of the estimated AoA values with respect to the GT values. The goal is to quantitatively measure how the obtained angles differ from the actual angles. We also measure the packet loss metric, which determines the percentage of beacons not received by the anchor nodes. As a significant example, concerning the MAE of the calibration scenario and on the azimuth plane, we range from a median value of $5.49°$ to $15.09°$, while for elevation plane, we vary from $6.95°$ to $16.80°$. Concerning the packet loss, it also varies according to the scenario and the anchor. As a significant example, we measure an average loss of 23% for the calibration scenario. The dataset is targeted to researchers and industry actors.

In summary, the main contributions of the paper are reported below:
- we collect and release to the community a dataset based on the Bluetooth 5.1 compliant specification, enabling the design and test indoor localization algorithms based on AoA and RSS techniques;
- the dataset allows modeling how AoA varies at realistic conditions. Not only, but the dataset also enables the design of simulators to quickly prototype and evaluate indoor localization algorithms;
- the dataset allows investigating the RSS variation with respect to the adopted channel, and based on the dual-polarized antennas' (1st and 2nd polarization);
- this work provides an analysis of the quality of the dataset based on the evaluation of the Mean Absolute Error between the collected data and the angles' GT, and an evaluation of the packet loss rate of anchor nodes. Furthermore, we study how RSS and AoA are influenced by the human body;
- we report some lessons we learned during the data collection campaign. The community can benefit of this experience for future deployments of similar hardware components.

The structure of this paper is the following. Section II surveys existing Bluetooth 5.1 datasets, Section III describes the testing environment and the design of the data collection campaign. The dataset format is reported in Section IV, while Section V reports the dataset analysis. Discussion and conclusions are reported in Section VII.

II. RELATED WORK

The current literature reports a limited number of datasets based on the Bluetooth 5.1 specification, and suitable for indoor localization systems.

Authors of [10] release a dataset based on a mathematical model of a non-uniform rectangular antenna array. The dataset is generated via a simulation process, considering a 8 patches antenna. The authors release two branches of the dataset: the first branch consists of 2.4 GHz pure sinusoidal tones used to obtain AoA samples, while the second branch adopts a baseband Bluetooth signals with constant tone extension (CTE), typical of the Bluetooth 5.1 specification. This synthetic dataset provides an interesting starting point to understand how AoA varies. Authors release not only the dataset, but also the Python code to generate the dataset so that to reproduce and modify the dataset. Moreover, the released dataset has been compared against with real IQ samples generated by a commercial transceiver prototype, adhering to the 5.1 specifications and equipped with an eight-sensors patch antenna array. This work mainly differs from [10] as we collect data with commercial hardware in a realistic indoor environment.

Authors of [11] release a Bluetooth 5.1 dataset specifically collected for indoor localization. The authors adopt four anchors equipped with an array of 8 antennas each and mounted using tripods in an indoor room of 100 m^2. Anchors

FIGURE 1: The indoor environment used for the data collection.

are deployed along the perimeter of the room, the target to be localized stands in 135 locations and authors also release the location's GT. The dataset has been used to evaluate an indoor localization algorithm, whose performance are detailed in [12]. This work moves toward our direction, however our data collection campaign includes a more extended set of scenarios (calibration, static, mobility and proximity) reproducing multiple emitters and multiple receivers at variable conditions. Other Bluetooth 5.1 datasets not specifically addressing the indoor localization are described in [13], [14]. We refer to [15]–[17] for more details about our previous works on the use of Bluetooth 5.1 for indoor localization based on preliminary data collection campaign based on 1 anchor node and 1 receiving node.

We summarize in Table 1 the main research studies on Bluetooth 5.1 in terms of dataset availability. It is worth noting that out of the surveyed works, only two of them also release a dataset to the community. Of them, we notice that one only has been designed to reproduce a realistic environment by means of commercial hardware. Furthermore, this particular study adopts only one receiver in a static scenario, evaluating the system in a limited number of fixed positions (135 positions). Differently, our dataset stands out as the only one that allows for the evaluation of multiple receivers simultaneously. The dataset includes data collected from 4 application scenarios with a variety of standing positions for each scenario. For these reasons, the proposed dataset offers a valuable opportunity to assess performance across a wide range of scenarios and receiver configurations.

III. EXPERIMENTAL DESIGN AND METHODS

We now describe the features of the testing environment that we adopted for the data collection. Our goal is to reproduce experiments in a realistic indoor environment, in which people are free to move and interact with other people.

To this purpose, we identify three key requirements driving the selection of the target environment:

1) An open and wide indoor environment suitable to reproduce a static positioning, a mobility and proximity scenario;
2) The existence of Wi-Fi networks reproducing typical environmental noise for indoor areas;
3) The possibility of deploying hardware components in the environment and of measuring the GT of the actual angles.

Given such requirements, we collect data in a wide open room located in our research institute, namely ISTI-CNR in Italy, as reported in Fig. 1. The room covers and area of 110 m^2, with the following dimension: 13.8x8 m and 3.1 m height. The floor is characterized by tiles of 60x60 cm, giving rise to a regular grid in which we can easily annotate the location's GT. With the term GT, we refer to the actual coordinates and timestamp of the target to localize, i.e. a person moving along a path, as reported in Section III-B. The room is covered by several Wi-Fi networks, this reproduces a realistic indoor setting. More specifically, we detect 46 Wi-Fi Access Points, of which 31 modulating at 2.5 Ghz and 15 modulating at 5 Ghz, respectively. During our tests, we did not receive signals from other Bluetooth networks.

A. SENSING INFRASTRUCTURE

Data are collected with the XPLR-AOA-1 kit produced by ublox, which includes anchor and tag nodes, as shown in Fig. 2. Anchor nodes are 11.5x11.5 cm boards provisioned with 5 C211 dual-polarized antennas, powered with the NINA-B411 micro-controller[1], and an USB port for I/O operations. The C209 tags are equipped with the NINA-B406 BLE module, supporting EddyStone beacon's format on 3 Bluetooth channels (37, 38 and 39). Tags can be configured to modify the advertisement rate, ranging from 1 to 50 Hz and the power of transmission, ranging from -40 dBm to 8 dBm.

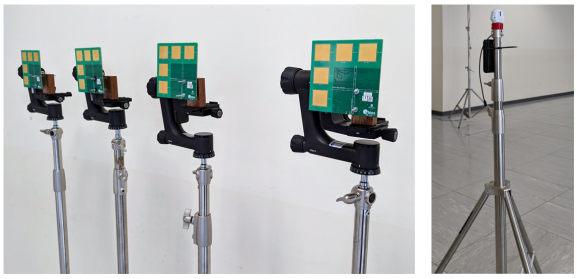

FIGURE 2: The adopted hardware for the data collection. Anchor nodes are mounted on top of a tripod with a professional head enabling an accurate orientation.

Anchor nodes are provisioned with custom firmware that we leveraged to log the following data:

- ϕ: the AoA between tag and receiver on the azimuth plane;
- δ: the elevation angle, the AoA between tag an receiver on a plane orthogonal to the azimuth plane;
- the Received Signal Strength (RSS) of 1st and 2nd polarization;

[1]https://www.u-blox.com/en/docs/UBX-20035327

TABLE 1: A comparison of existing works based on AoA for Indoor Localization.

Reference	Year	Hardware	Anchors	Tags	Environment [m]	Tested Locations	Scenario	Dataset avail
[18]	2021	SLWSTK6006A	4	1	25x15	8	static	no
[19]	2022	BOOSTXL-AOA	2	1	5x5	4	static	no
[15]	2022	XPLR-AOA-1	1	1	14x8	112	static	no
[16]	2023	XPLR-AOA-1	1	1	14x8	112	static	no
[17]	2023	XPLR-AOA-1	1	1	14x8	112	static	no
[10]	2021	simulation	1	1	n.a	n.a	n.a	✓
[11]	2021	custom hardware	1	1	12.5x8	135	static	✓
our solution	2023	XPLT-AOA-1	4	4	14x8	356	calibration, static, mobility, proximity	✓

- the advertisement Bluetooth channel used by the tag (37, 38, 39);
- the timestamp tracking the up-time of the logging node.

Anchors nodes are connected via USB to a Raspberry PI board. The Raspberry board stores data logged by anchors on a memory support, for post-processing analysis. Anchors estimate azimuth angle ϕ and elevation angle δ in the range $-90° \leq (\phi, \delta) \leq 90°$ with 2° of angle resolution.

When considering real-time scenarios, in which it becomes necessary to immediately estimate the target's position, then the anchor's logging messages (containing the azimuth and elevation values) can be published via MQTT (Message Queuing Telemetry Transport) protocol to a MQTT broker. The localization service, which is responsible for estimating the position, subscribes to this MQTT broker to receive a stream of messages and it can run a specific algorithm to estimate the target's position.

B. REFERENCE SCENARIOS AND GROUND TRUTH ANNOTATION

We test and collect data with the corresponding GT in four application scenarios, as detailed in the next:

- *Calibration*: data are collected from four anchors and 1 tag mounted on a tripod and positioned in 119 different locations of the testing environment. The calibration scenario is suitable to study how AoA and RSS vary at *stable* and reproducible conditions. The 119 locations evenly cover the whole testing environment.
- *Static*: data are collected from four anchors and 1 tag held by a person resting in 36 different locations. The tag is locked on a lanyard around the person's neck; we collect data with the person oriented toward North, South, East and West to enable the study of body effect to the collected data.
- *Mobility*: data are collected from four anchors and a person holding the tag around the neck. This scenario includes three use-cases, each characterized by a different mobility. Each use-case has been repeated for 4 runs. This scenario is designed to enable the study of indoor localization algorithms with a moving target.
- *Proximity*: the goal is to collect data from four anchors while people get in proximity. We reproduce the formation of dyads, triplets and of groups of 4 people approaching and distancing along the time. Each person holds a tag locked around the neck.

Concerning the Calibration scenario, we report in Fig. 3 the layout of the grid and the 119 reference locations. The figure shows the location of anchor nodes which are referred to with labels: $6501, 6502, 6503, 6504$. Anchors are mounted on top of a tripod at 2.3 m from the ground and oriented with a professional head, which enables an accurate orientation of the anchor. In all the experiments, the azimuthal plane of the anchors is parallel to the floor as shown in Fig. 2.

The grid is spaced by 60 cm, and the dataset also includes the actual angles between the tag and four anchor nodes, for each of the 119 locations. The tag is always positioned on top of a tripod oriented toward East at 1.10 m from the ground. The tag advertises beacons at 50 Hz with a power of emission set to 0 dBm. The tag rests in each of the 119 locations for 1 minute.

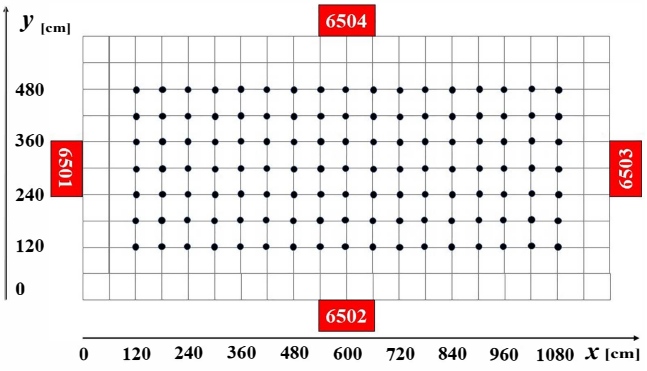

FIGURE 3: Use-case of the Calibration scenario.

Concerning the Static scenario, we involve a person holding a tag around the neck and resting for 1 minute in each of the 36 reference locations as reported in Fig. 4. With this scenario, we can reduce the number of reference location, one each 120 cm. Moreover, we replicate the same scenario using 4 different orientations of the person: North, South, East and West.

Concerning the Mobility scenario, we consider three use-cases. Similarly to the other scenarios, a person holds a tag around the neck as reported in Fig. 5. We reproduce three use-cases, each repeated for 4 runs. In all of them, the person

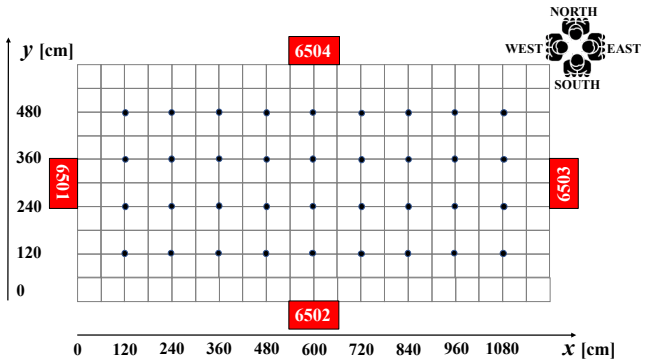

FIGURE 4: Use-case of the Static scenario.

moves with a pedestrian speed of about 0.5 m/s. In particular, with use-cases 1 and 2 the person does not stop while walking along the paths. Differently, with use-case 3-case the person stops in some stay-locations for 1 minute, after that she keeps moving towards the end of the path.

Lastly, concerning the Proximity scenario we define 4 proximity use-cases, as reported in Fig. 6. With the term proximity we refer to an event in which a person gets close to a point of interest or to another person. The 4 proximity settings cover several use-cases and they reported in the following:

1) Proximity 1: a person holds the tag around the neck while getting in proximity of 5 POIs. The person rests for 2 minutes in each POI and them he/she moves to the next POI;
2) Proximity 2: a group of 4 people get in proximity for 2 minutes and then they move away. All the people hold the tag around the neck;
3) Proximity 3: a group of 3 people get in proximity, while another person is isolated;
4) Proximity 4: 2 groups of 2 people get in proximity

Each of the 4 proximity use-cases are repeated for four iterations, so that to have multiple runs for the same use-case.

The 4 scenarios give rise to an extended data collection campaign, resulting with more than three millions samples over three hours of data collection. Table 2 provides details concerning the amount of the collected data for each scenario and the duration. It is worth noticing that the amount of collected values are lower than what the theoretical value. More specifically, we observe for each scenario a certain packet loss rate, defined as the percentage of beacons not collected by any of the four anchors. This loss is caused by several factors: wireless interference, hardware failures, firmware errors during the data collection, as measured in Table 9.

For all the mentioned scenario, GT correspond to the actual location of the tag (coordinates on the grid) and the corresponding timestamp. To this purpose, we adopt an Android-based mobile application, namely *StepLogger*, as described in our previous work [20]. StepLogger implements an intuitive GUI showing a button labeled with a custom string. Strings, typically, correspond to markers on the ground positioned in the reference locations. As soon as a person steps over a reference location, he/she presses the button and StepLogger logs the corresponding string, x,y coordinates and the timestamp (expressed as UNIX timestamp). We publicly release the StepLogger application to the community under the Apache 2.0 license [2].

TABLE 2: Dataset overview.

Scenario		Labeled Positions	Collected Values	Duration [min.]
Calibration		119	1 098 620	119.98
Static	North	36	349 853	40.09
	West		339 568	38.89
	East		338 235	38.85
	South		332 290	37.85
Mobility	use-case 1	16	32 420	3.66
	use-case 2	10	19 028	2.14
	use-case 3	16	170 504	19.55
Proximity	use-case 1	5	94 314	10.94
	use-case 2	-	229 600	18.94
	use-case 3	-	226 731	18.71
	use-case 4	-	224 505	18.56
Total			**3 455 668**	**368.16**

C. ENVIRONMENTAL SETUP

We report in this section some details concerning the effort required to setup the testing environment. The dataset has been collected in an empty room, and we perform the following operations:

- Determining the reference system for anchors' and users' locations;
- Deploying anchors;
- Determining the ground truth.

Concerning the first point, we exploit the shape of the floor to determine a reference system. More specifically, the floor is composed of 60x60 cm tiles, forming a regular grid. Therefore, it is relatively easy to determine any location inside the room, using a relative reference system. To this purpose, we set the $(0, 0)$ point on the lower-left corner of the environment, as reported in Fig. 3. Concerning the anchors' deployment, we test various settings (as also detailed in [15]–[17]). We decide to deploy two anchors on the long-side of the environment and two anchors on the short-side for two reasons:

1) maximizing the anchor's coverage;
2) adopting a reproducible setup.

Indeed, other possible deployments consist of attaching anchors on the ceiling (parallel with the respect to the floor), but such setup requires a non-negligible effort and a specific equipment to correctly deploy anchors, without a net improvement of the performance. In our case, we adopt a tripod with a professional head mounted on top of it, which

[2]https://github.com/wnlab-isti/steplogger_fullscreen

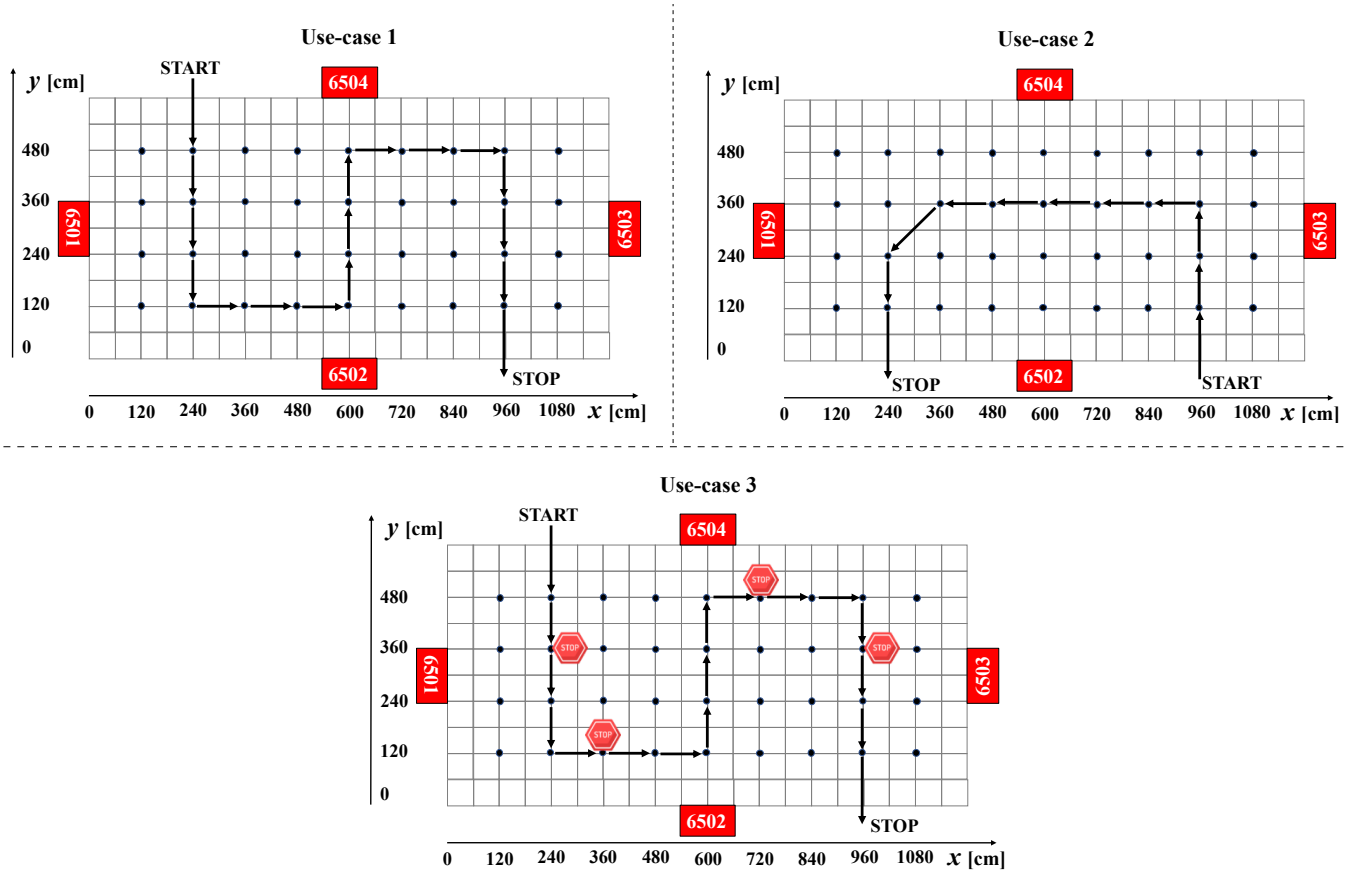

FIGURE 5: Use-cases of the Mobility scenario.

allows us to easily position anchors on the x, y and z axis. Lastly, concerning the GT, we annotate the timestamp and the location of the tag for all the testing scenarios. The location can be easily obtained with the reference system previously described (tiles of 60 cm on a regular grid), the timestamp is obtained with a simple Android application, namely StepLogger, as described in Section III-B.

IV. DATASET FORMAT AND AVAILABILITY

The dataset described in this work is available to the community [9] and it is organized with four folders one for each scenario: Calibration, Static, Mobility and Proximity. Each folder contains the sub-folders `beacons` and `gt`, with raw data and the GT, respectively. The raw data are timeseries of values, each row reports values logged by an anchor node. The raw data format is shown in Table 3, all fields are numeric values with the following meaning:

- `EpochTime`: receiving beacon message time;
- `Tag ID`: Bluetooth tag identifier;
- `RSS 1st polarization`: RSS value of the 1st polarization;
- `AoA Az.`: AoA value on the azimuth plane estimate by the anchor;
- `AoA El.`: AoA value on the elevation plane estimate by the anchor;
- `RSS 2nd polarization`: RSS value of the 2nd polarization;
- `Channel`: the Bluetooth channel used by the anchor to receive the beacon message;
- `Anchor ID`: the ID of the anchor node.

Concerning the GT annotation, the dataset fields are shown in Table 4. The GT data format varies according to the scenarios as detailed in the following:

- *Calibration* and *Static*: the meaning of fields in Table 4 is the following:
  - `Start time`: the timestamp the tag arrives in a specific position;
  - `End time`: the timestamp the tag leaves a specific position;
  - `GT x-axis`: the x-coordinate of the tag's location;
  - `GT y-axis`: the y-coordinate of the tag's location;
- *Mobility* and *Proximity, use-case 1*: the meaning of the fields in Table 4 is the following:
  - `Start time`: the timestamp the tag arrives in a specific position;
  - `End time`: this field can be ignored for use-cases 1 and 2 of the mobility scenario. This field

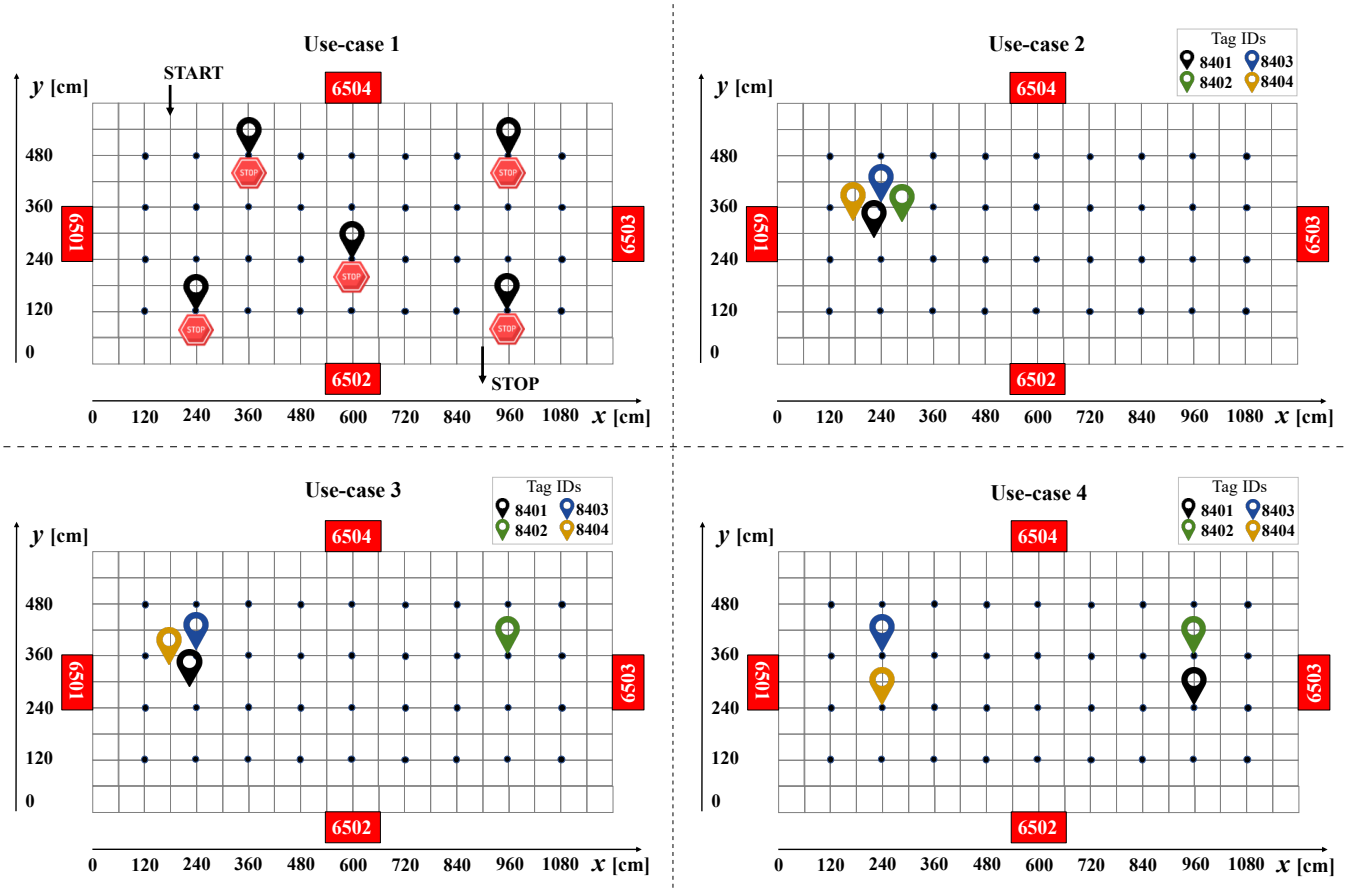

FIGURE 6: Use-cases of the Proximity scenario.

TABLE 3: Data format of values logged by anchor nodes.

EpochTime	Tag ID	RSS 1st pol.	AoA Az. (ϕ)	AoA El. (δ)	RSS 2nd pol.	Channel	Anchor ID

TABLE 4: Data format of GT annotations.

Start time	End time	GT x-axis	GT y-axis

reports the leaving time of the person from the stop-location for use-case 3;
  - `GT x-axis`: the x-coordinate of the tag's location;
  - `GT y-axis`: the y-coordinate of the tag's location;
- *Proximity, use-cases 2,3 and 4*: the meaning of fields reported in Table 4 is the following:
  - `Start time`: the starting time of the proximity event in a specific position;
  - `End time`: for the ending time of the proximity event in a specific location
  - `GT x-axis`: this field can be ignored;
  - `GT y-axis`: this field can be ignored;

The dataset also includes details of the grid of 119 locations used for the experiments, see Fig. 3. The file named `grid_details` reports for every location the actual angles with four anchor nodes according to the following format:

- `X`: x-coordinate of the location;
- `Y`: y-coordinate of the location;
- `AoA az.`: actual angle on the azimuth plane between the tag and the anchor with respect to the current location;
- `AoA el.`: actual angle on the elevation plane between the tag and the anchor with respect to the current location;
- `Anchor ID`: ID of the anchor.

V. EXPERIMENTING WITH THE DATASET

We now analyze the dataset with the goal of highlighting some key aspects useful to better understand how AoA and RSS vary in the experimental scenarios. We first describe how we determine the angles' GT and then we describe the considered evaluation metrics to measure the quality of the dataset.

TABLE 5: Settings for determining the range of ϕ and δ for anchor 6501.

	Azimuth Angle ϕ		Elevation Angle δ	
	Min. Value	**Max. Value**	**Min. Value**	**Max. Value**
Z_T	110	110	110	110
Z_A	230	230	230	230
X_T	120	120	120	1080
X_A	0	0	0	0
Y_T	480	120	300	120 to 480
Y_A	300	300	300	300

TABLE 6: Settings for determining the range of ϕ and δ for anchor 6502.

	Azimuth Angle ϕ		Elevation Angle δ	
	Min. Value	**Max. Value**	**Min. Value**	**Max. Value**
Z_T	110	110	110	110
Z_A	230	230	230	230
X_T	120	1080	600	120 or 1080
X_A	600	600	600	600
Y_T	120	120	120	480
Y_A	0	0	0	0

A. COMPUTING THE GROUND TRUTH

Before presenting our analysis, we detail the geometrical process to obtain the angle's GT that we use to compute the MAE. It is worth to notice that the resolution of the anchor nodes is 2°. More specifically, each anchor estimates the angle of arrival of tag's messages with 2° of possible inaccuracy.

The GT of the elevation angle δ is obtained for all the anchors as follows:

$$\delta = \arctan\left(\frac{z_T - z_A}{\sqrt{(x_T - x_A)^2 + (y_T - y_A)^2}}\right) \quad (1)$$

where (x_A, y_A, z_A) and (x_T, y_T, z_T) are the coordinates of the anchor and the tag, respectively. Differently, the GT of the azimuth angle is computed based on the position of the anchor. More specifically, for anchors 6501 and 6503 which have been positioned on the room's short sides, the GT azimuth angle is obtained as follows:

$$\phi_{(6501,6503)} = \arctan\left(\frac{y_A - y_T}{x_T - x_A}\right) \quad (2)$$

while for anchors 6502 and 6504, which have been located on the room's long sides, we calculate the GT azimuth angle as follows:

$$\phi_{(6502,6504)} = \arctan\left(\frac{x_A - x_T}{y_A - y_T}\right) \quad (3)$$

We report in Fig. 7 the GT of the azimuth ϕ (blue color) and elevation δ (black color) of the angles for anchors 6501 and 6502 (same values are for anchors 6503 and 6504, as they are symmetrical). In particular, the range of the expected angles on the azimuth plane are computed according to 2 and 3 giving the following ranges: $-56° \leq \phi \leq 56°$ for anchors 6501 and 6503, and from $-76° \leq \phi \leq 76°$ for anchors 6502 and 6504. Concerning the elevation plane δ, the range is obtained with 1 giving the following ranges: $-45° \leq \delta \leq -6°$ for anchors 6501 and 6503, and $-45° \leq \delta \leq -10°$ for anchors 6502 and 6504. Settings for determining the range of ϕ and δ for anchors 6501 and 6502 are reported in Tables 5 and 6, respectively.

B. RESULTS

We analyze the dataset to measure the quality of the collected data. In particular, we compute the following evaluation metrics:

- the Mean Absolute Error (MAE) computed between the angle's GT (ϕ, δ) and the estimated angles ($\hat{\phi}$, $\hat{\delta}$) for the calibration scenario;
- the packet loss for each scenario as the amount of Bluetooth beacons not recorded by the four anchors;
- the RSS distribution and the corresponding impact of the human body, of the adopted Bluetooth channel and of two antenna's polarizations;
- the AoA distribution and the corresponding impact of the human body.

We now compare the GT with estimated angles by computing the Mean Absolute Error (MAE) as follows:

$$\text{MAE}_\phi = \frac{\sum_{i=1}^{n} |\phi_i - \hat{\phi}_i|}{n}; \text{MAE}_\delta = \frac{\sum_{i=1}^{n} |\delta_i - \hat{\delta}_i|}{n} \quad (4)$$

where n is the number of collected samples for a given location. Concerning the calibration scenario, we show in figures 8 and 9 the contour map of the MAE, obtained both on the azimuth and elevation planes. We report a map for each of the four anchors. The color bar of the maps ranges from 0° to 30°. From the figures, we observe that the MAE varies in the grid. We can identify regions characterized by low values of the MAE, and regions with high values of the MAE such as the peripheral regions with anchors 6502 and 6504 in Fig. 8. As a general trend, we observe that the MAE varies in a different way when considering anchors deployed on the short or long side of the environment. More specifically, anchors 6502 and 6504 differ with respect to anchors 6501 and 6503. In the first case, anchors are located on the long side of the room and we observe a confidence region with low values of the MAE in the range $-45° \leq \phi \leq 45°$. Such a region fits with a triangular shape centered in the anchor coordinates and expands towards the center of the room. This behaviour is particularly evident for the azimuth measurements (Fig. 8). Outside this range, the MAE increases until its maximum, mainly at the corner locations. On the second case, anchors (6501 and 6503) are located on the short side of the room and we are not able to identify a clear pattern of MAE variation. Moreover, we analyze the difference between the MAE computed on the azimuth and elevation plane. From our analysis, values of MAE computed on the elevation plane are generally higher than that of the azimuth plane. This pattern can be observed from the yellow regions reported in the contour map of Fig. 9.

Tables 7 and 8 report the median and 75th percentile of the MAE for azimuth and elevation angles, respectively, for

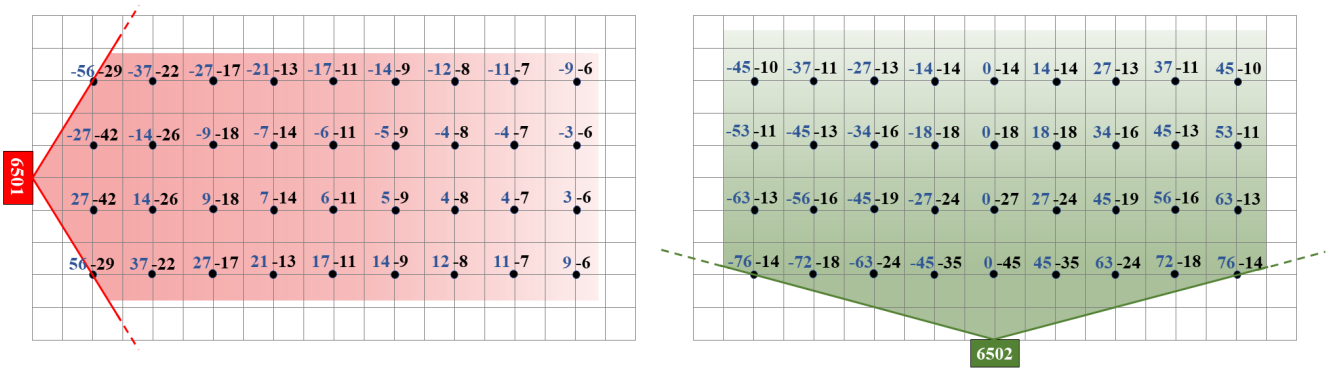

FIGURE 7: We report the expected azimuth ϕ (in blue colour) and elevation δ (in black colour) angles, for each 36 locations and for anchors 6501 and 6502.

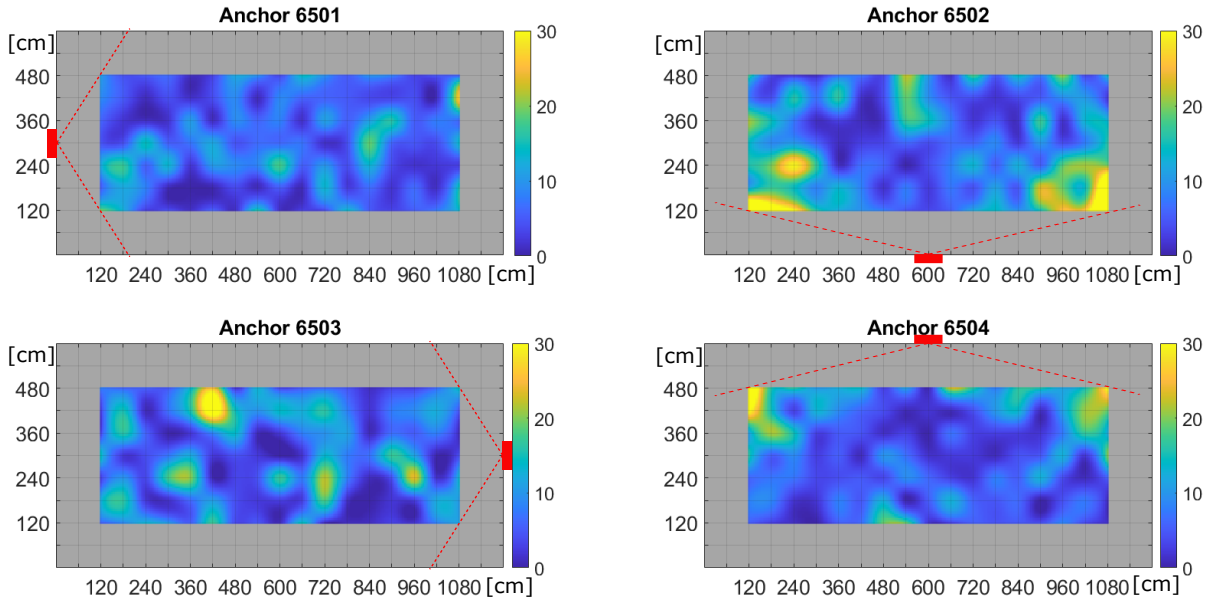

FIGURE 8: MAE of azimuth angle ϕ of the four anchor nodes. Color bar reports the error range expressed in degree.

the calibration and static scenarios. Concerning the azimuth, the median values range from 5.22° (Anchor 6501, Static West) to 21.35° (Anchor 6504, Static South). Furthermore, we observe that the minimum error values are obtained when the person is oriented in line-of-sight with the anchor. In particular, anchor 6501 achieves the minimum error with west orientation (median value of 5.22°), Anchor 6502 with south orientation (median value of 6.04°), anchor 6503 with east orientation (median value of 5.32°), and anchor 6504 with north orientation (median value of 6.65°). Similar considerations can be made for the elevation angle. However, we note higher median errors across all scenarios, ranging from 5.77° (anchor 6504, Calibration scenario) to 21.33° (anchor 6504, Static South scenario).

The second analysis we report in this work refers to the packet loss rate, that we compute for all the scenarios. The packet loss measures the amount of beacons not received by anchor nodes. The expected number of beacons can be calculated, because the tag's advertisement frequency (set to 50 Hz) and the duration of the experimental scenario are known. Table 9 reports the packet loss rate. As reported in the table, the loss rate ranges from 22.61% to 74.89%, depending on the scenario: concerning scenarios with only one transmitter, the loss rate does not exceed 30.36%. Differently, by increasing the number of tags, the loss rate also increases exceeding 74%: it is the case of Proximity scenario, use-cases 2,3 and 4. In these cases the listening frequency of the tags is inversely proportional to the number of tags. In other words, as the number of tags increases, the frequency at which they are listened to decreases. Generally, when tracking a person, we aim to estimate their position at a minimum frequency of 1 Hz. This means that theoretically, the system could track a maximum of 50 people, considering the maximum frequency of 50 Hz. In the experiment room of 110 m, e.g. size of an exhibition room of a museum, this would correspond to a crowded environment with an average interpersonal distance

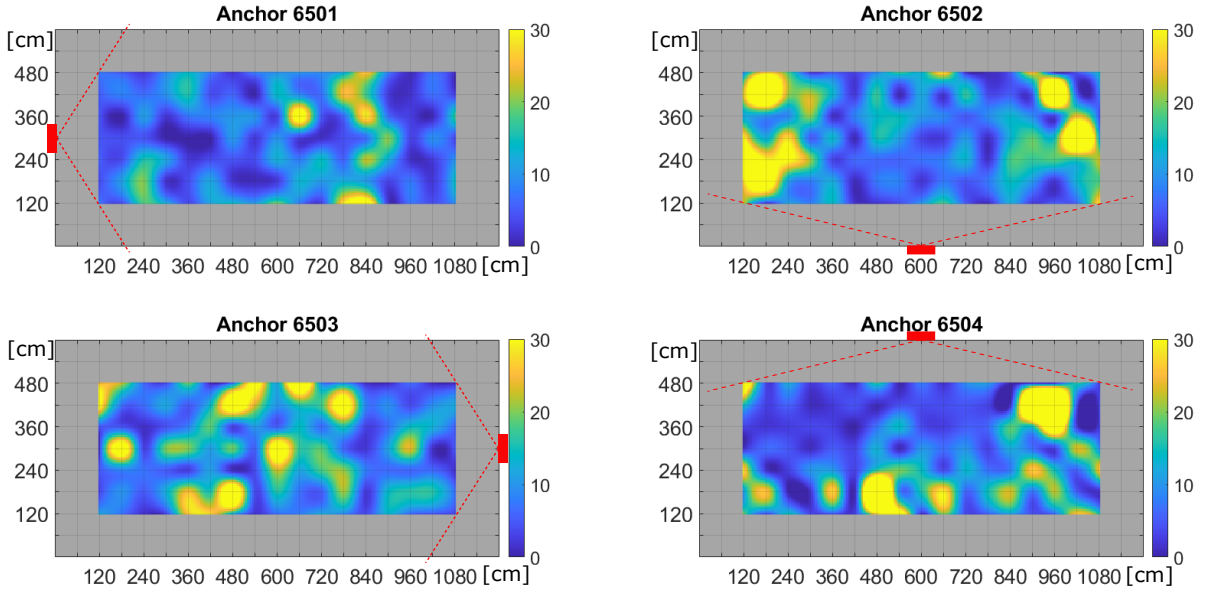

FIGURE 9: MAE of elevation angle δ of the four anchor nodes. Color bar reports the error range expressed in degree.

TABLE 7: Median and 75th percentile of Azimuth MAE for Calibration and Static scenarios, for all the anchors.

Scenario		**Anchor 6501**		**Anchor 6502**		**Anchor 6503**		**Anchor 6504**	
		median	75th	median	75th	median	75th	median	75th
Calibration		5.49	9.23	8.24	15.09	6.10	11.96	5.50	11.40
Static	North	14.92	19.92	10.45	15.02	8.45	13.52	6.65	14.09
	West	5.22	8.94	7.07	14.33	13.42	19.60	12.54	17.29
	East	8.38	14.38	9.09	14.54	5.32	9.34	7.77	16.46
	South	10.77	13.35	6.04	9.23	11.58	15.74	21.35	34.28

TABLE 8: Median and 75th percentile of Elevation MAE for Calibration and Static scenarios, for all the anchors.

Scenario		**Anchor 6501**		**Anchor 6502**		**Anchor 6503**		**Anchor 6504**	
		median	75th	median	75th	median	75th	median	75th
Calibration		6.95	10.82	9.93	16.80	8.40	15.92	5.77	14.76
Static	North	13.77	17.94	12.51	17.59	11.81	18.25	10.23	17.57
	West	9.97	15.79	14.79	23.82	13.62	25.96	18.00	28.95
	East	14.17	21.15	14.23	25.44	10.89	15.72	14.01	28.91
	South	12.47	16.30	8.05	15.49	15.51	22.20	21.33	28.17

of approximately 80 cm. However, it's important to note that in such cases, the accuracy of the location degrades significantly.

Furthermore, concerning the Static scenario, we note that the body orientation has an impact on the packet loss. More specifically, the anchor 6501 achieves its maximum loss rate with the person's body oriented towards the East, meaning when the person is oriented on the opposite side of the anchor 6501. We can make the same considerations for anchors 6502, 6503, and 6504 with north, west, and south orientations, respectively.

We also analyze the impact of the body to the RSS distribution. More specifically, we compare data collected with the Calibration scenario, in which a tag is mounted on top of a tripod oriented towards East, with respect to the Static scenario, in which a person holds a tag around the neck with the same orientation. Moreover, we compare data by using the 36 locations of the Static scenario, see Fig. 4 so that to reduce the complexity of the resulting graphs without loosing features of the RSS distribution. Fig. 10 shows the resulting comparison. The figure shows for every location and for every anchor node (6501 to 6504) a pair of boxplots, one for the Static (white color) and one for the Calibration (red color) scenarios. From the figure, we observe that distributions obtained with the Static scenario tend to extend more significantly with respect to the Calibration scenario, as the human body introduces a source of noise for the collected data. This pattern can be observed with locations $(240, 480)$, $(1080, 480)$, $(960, 120)$. It is worth to notice that the previous analysis is obtained by filtering RSS samples collected on

TABLE 9: Packet loss rate for all the scenarios and anchors.

Scenario		Anchor 6501	Anchor 6502	Anchor 6503	Anchor 6504
Calibration		22.61	23.50	24.49	24.21
Static	North	28.26	27.06	26.81	26.66
	West	25.48	25.72	29.83	27.97
	East	29.76	26.86	25.93	27.28
	South	26.64	25.76	26.64	28.34
Mobility	use-case 1	25.75	25.99	26.17	26.84
	use-case 2	25.18	24.98	26.14	27.08
	use-case 3	26.93	27.55	26.22	28.55
Proximity	use-case 1	26.19	30.36	28.16	27.89
	use-case 2	74.62	74.70	74.86	74.81
	use-case 3	74.71	74.74	74.75	74.82
	use-case 4	74.68	74.89	74.75	74.89

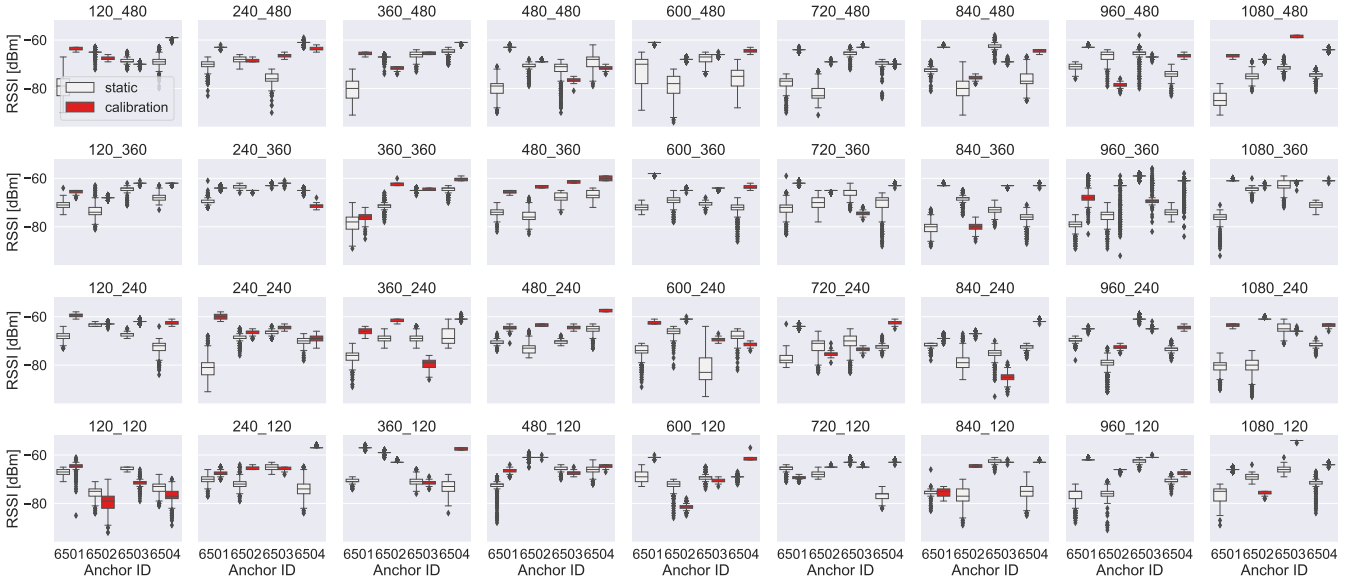

FIGURE 10: Comparison of RSS distributions between Static and Calibration scenarios.

a single Bluetooth channel, namely channel 39. Indeed, we observe that the 3 available Bluetooth channels (37, 38 and 39) have a different impact to the resulting RSS distributions. We further investigate this aspect in Fig. 11, analysing all the RSS values collected in the static scenario for all 36 positions. This figure clearly shows how filtering data on different channels affect the resulting distributions.

Still concerning the RSS values on the Calibration scenario, we show for each of the 36 locations how RSS varies on both 1st and 2nd polarization for every anchor node. Results of this comparison are reported in Fig. 12. In certain specific locations, such as the $(120, 480)$ anchors 6502 and 6503, as well as the $(1080, 120)$ anchor 6503, the distributions of RSS values for the two polarizations are comparable. However, this similarity in distributions is not present throughout the majority of locations tested, where a remarkable difference is present between the two polarizations in terms of their RSS values. This difference in RSS values can be attributed to the effects of antenna's polarization; indeed, antenna's polarization is one of the most crucial factors that impact the RSS. As a result, it is expected that there would be a noticeable discrepancy in the RSS values of the two polarizations, especially when observed across a vast range of locations. Additionally, it can be inferred that locations with comparable distributions of RSS values across polarizations may have similar characteristics that mitigate the impact of polarization on RSS. More information about antenna's polarization for indoor localization are reported in [21], [22].

We lastly analyze AoA distributions both on the azimuth and elevation planes by comparing the Static and the Calibration scenarios, as done with Fig. 10. More specifically, we measure the impact of the body to the estimated AoA values from the four anchors. Fig. 13 reports for each location and for each anchor a pair of boxplots, one for the Static (orange color) and one for the Calibration (green color) scenarios. Similarly to the RSS distributions, the Static scenario introduces a certain degree of inaccuracy for the AoA values on the azimuth plane. The first observation is that estimated AoA values are generally constrained in a small interval, e.g. 2°

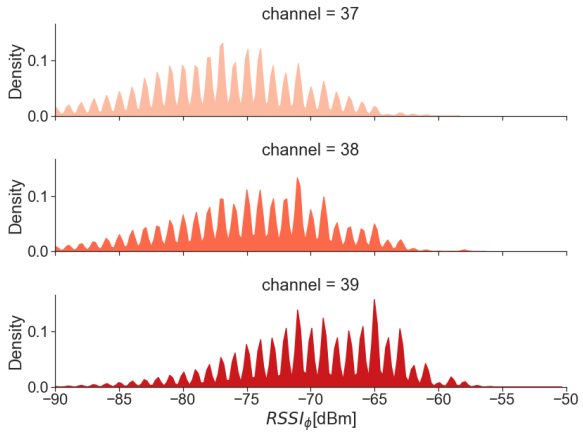

FIGURE 11: Impact of the Bluetooth channel to the RSS distribution.

to 10°. The second observation is that with the Calibration scenario such interval is even smaller than that of the Static scenario, in which the human body has a negative effect, as observable with locations: $(240, 480)$ and $(1080, 240)$.

VI. LIMITS OF THE BLUETOOTH TECHNOLOGY

The data collection described in this work allowed us to face with the limits of the Bluetooth 5.1 specification. We report in this section some final considerations about its practical use. In particular, we discuss two main issues: wireless interference and the line-of-site requirement.

Concerning the first issue, we consider that wide indoor environments present unique challenges for Bluetooth coverage. These environments are characterized by complex layouts, multiple rooms, and various obstacles that can impede the transmission of Bluetooth signals. Such obstacles can adversely affect the range of Bluetooth signals. Nevertheless, it is important to note that most of the wireless technologies suitable for indoor applications, including Wi-Fi and UWB, also have inherent limitations in terms of range. Indeed, these technologies often require additional infrastructures to effectively cover wide areas. More specifically, we refer to the strategic deployment of multiple anchor nodes, e.g. positioned on the ceiling. Differently from simulation approaches, our dataset focuses on reproducing real-world conditions. We deliberately avoid selecting interference-free environments and we opted for deploying multiple anchor nodes in the testing environment, so that researchers and developers can assess the performance and robustness of AoA-based systems in practical scenarios.

Concerning the second aspect, namely the non-line-of-sight issue, we argue that most of the Radio Frequency technologies are affected by the multipath propagation problem. In order to mitigate non-line-of-site conditions, the dataset we describe in this work is obtained by deploying four anchor nodes, evenly covering the environment and enabling researchers to mitigate those situations in which the Bluetooth tag is not in line-of-sight with one or more anchor nodes. Large scale deployment sites based on the Bluetooth technology, can be properly designed: by increasing the number of anchors or by deploying anchors in locations with high visibility regions, e.g. mounted on the ceiling.

VII. DISCUSSION AND CONCLUSION

Indoor localization systems have been increasing their accuracy also thanks to the adoption of AoA technologies able to estimate the direction of an indoor target. In this work, we detail a data collection campaign based on Bluetooth 5.1 Direction Finding specification. We collect data from four anchor nodes deployed in a wide-open room of 110 m^2, and we reproduce four experimental scenarios of increasing complexity. Collected data include Angle of Arrival, RSS values, timestamp and a GT annotation.

The dataset is publicly available to the community [9]. This dataset provides three main lines of investigation.

Firstly, the dataset can be used to design and test indoor localization algorithms exploiting AoA and RSS. Indeed, it is possible to design algorithms estimating the location by triangulation/trilateration [23] and filtering techniques, as the collected data also include estimated angles from all anchor nodes simultaneously. The collected RSS values can be used in conjunction with AoA values. Indeed, on the one hand, RSS can be used to estimate the distance from an anchor by adopting a path-loss model, while on other hand AoA provides the estimated orientation towards such anchor. The RSS values released with this dataset also include the adopted Bluetooth channel (channels 37, 38 and 39), and the influence of the 1st and 2nd antenna's polarization. Such information is useful for testing RSS-based algorithms and comparing their performance across different channels.

Secondly, the dataset could be employed to study how AoA varies in space and at different conditions. Indeed, the Calibration and Static scenarios that we reproduce collect data at unchanged conditions, thus this data could be employed to design an anchor's model.

Lastly, the design method reported in Section III offers to readers some lessons we learned for a successful data collection campaign. More specifically, we identify a set of requirements for the data collection, leading to a realistic and representative setting. Concerning the presence of wireless interferences operating at 2.5 GHz, they might introduce a certain degree of noise in the environment. We argue that such noise might, in certain cases, lead to the corruption of Bluetooth packets, for example in such situations in which the interfering signals corrupt a Bluetooth message. To this purpose, the packet loss metric, that we show in Table 9, provides an overall quantification of the beacon messages not received by each of the four anchors. It is worth noting that the packet loss metric also includes events in which the Bluetooth anchors miss a message for other reasons, i.e. hardware failure. Differently from the packet loss metric, the environmental noise does not affect the estimated values of the AoA. Indeed, the Bluetooth anchors process a message

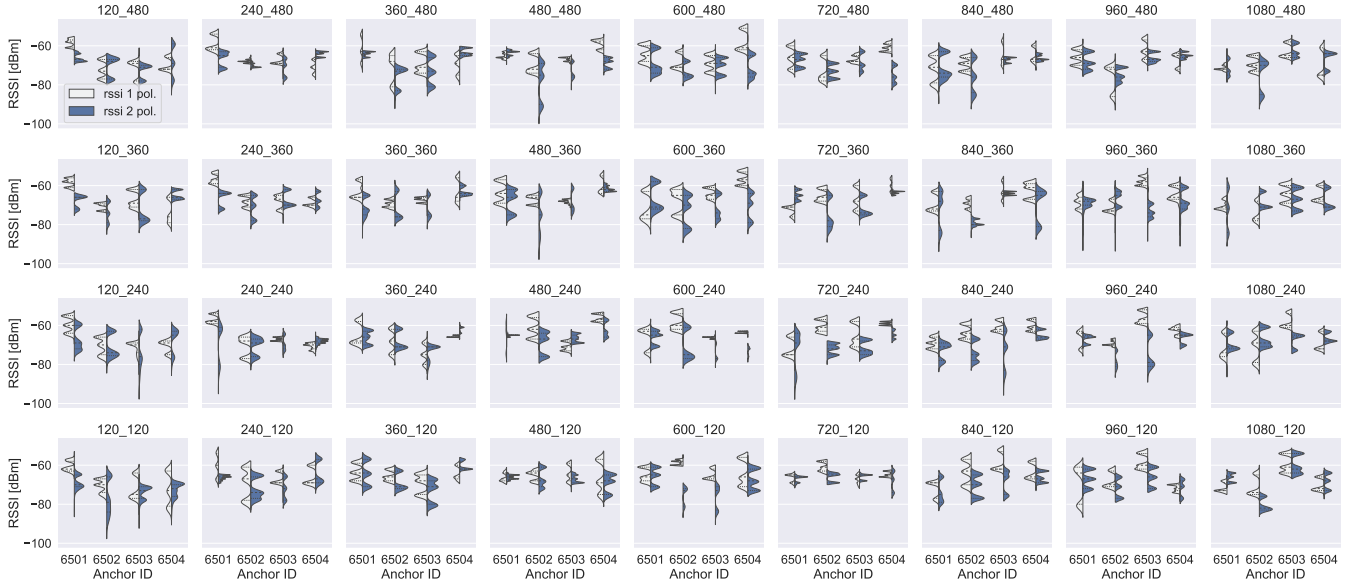

FIGURE 12: RSS distributions obtained with using RSS values of the 1st and 2nd polarization.

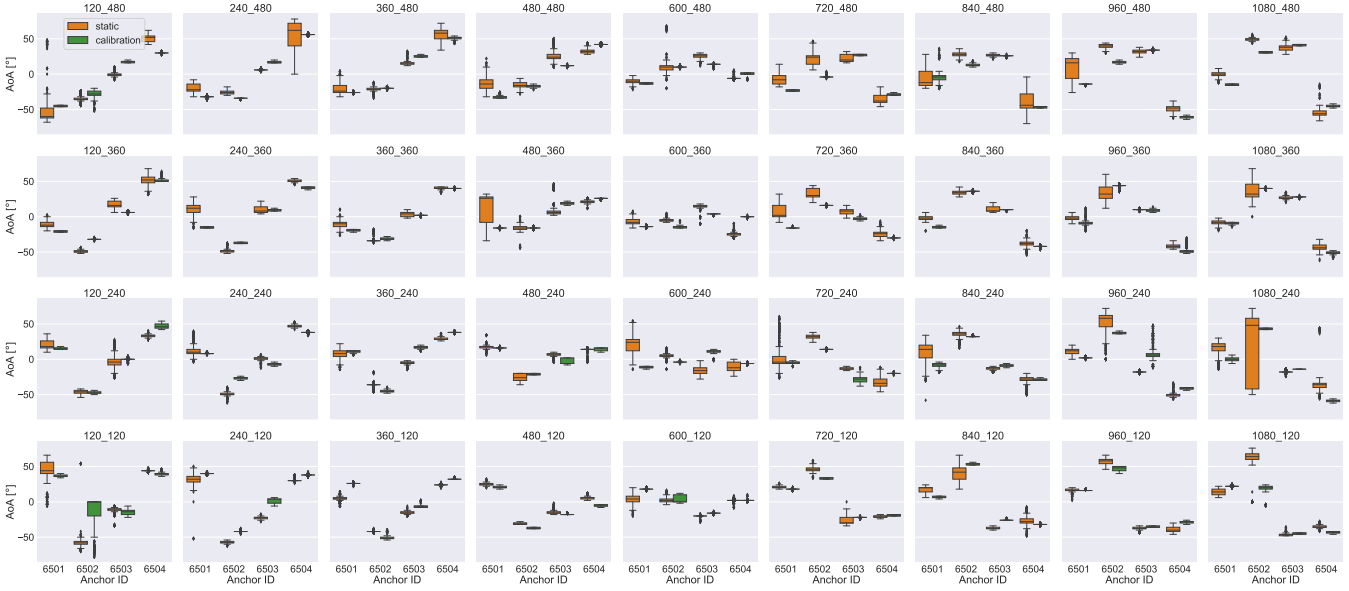

FIGURE 13: Comparison of AoA distribution on the azimuth plane between Static and Calibration scenarios.

only when not corrupted: preamble and payload frame are correctly received.

We expect that Direction Finding specification will be readily available with commercial devices. Initially, software updates can enable smartphones and smartwatches to function as radio beacons, emitting messages compliant with the Bluetooth 5.1 specification. Alternatively, radios can be updated to distinguish the phases of messages emitted using antenna arrays deployed in the environment. In the first case, mobile devices can be utilized as Bluetooth tags, with the infrastructure estimating the device's position using AoA techniques. In the second case, the mobile device itself can estimate the position using AoD techniques or enable navigating towards reference points. Ultimately, the design of new antenna arrays specifically tailored for smartphones will allow the adoption of specular solutions in positioning [24], [25].

A last consideration refers to the privacy of the monitored users. The effectiveness of an indoor localization system is greatly influenced by the adopted technologies to estimate the position of a target in an indoor environment. No dominant technological solution has emerged so far, and widespread commercial deployment will only be possible by addressing privacy concerns [26].

REFERENCES

[1] C. Laoudias, A. Moreira, S. Kim, S. Lee, L. Wirola, and C. Fischione, "A survey of enabling technologies for network localization, tracking, and navigation," *IEEE Communications Surveys & Tutorials*, vol. 20, Art. no. 4, pp. 3607–3644, 2018.

[2] F. Zafari, A. Gkelias, and K. K. Leung, "A survey of indoor localization systems and technologies," *IEEE Communications Surveys & Tutorials*, vol. 21, Art. no. 3, pp. 2568–2599, 2019.

[3] W. M. Gifford, D. Dardari, and M. Z. Win, "The impact of multipath information on time-of-arrival estimation," *IEEE Transactions on Signal Processing*, vol. 70, pp. 31–46, 2022.

[4] Y. Xu, Y. S. Shmaliy, Y. Li, and X. Chen, "Uwb-based indoor human localization with time-delayed data using efir filtering," *IEEE Access*, vol. 5, pp. 16 676–16 683, 2017.

[5] Q. Liang and M. Liu, "An automatic site survey approach for indoor localization using a smartphone," *IEEE Transactions on Automation Science and Engineering*, vol. 17, Art. no. 1, pp. 191–206, 2020.

[6] N. Paulino and L. M. Pessoa, "Self-localization via circular bluetooth 5.1 antenna array receiver," *IEEE Access*, vol. 11, pp. 365–395, 2023.

[7] A. Bensky, "Chapter 14 - technologies and applications," in *Short-range Wireless Communication (Third Edition)*, third edition ed., A. Bensky, Ed. Newnes, 2019, pp. 387–430. [Online]. Available: https://www.sciencedirect.com/science/article/pii/B9780128154052000142

[8] K. Witrisal, C. Anton-Haro, S. Grebien, W. Joseph, E. Leitinger, X. Li, J. A. Del Peral-Rosado, D. Plets, J. Vilà-Valls, and T. Wilding, "Chapter 9 - localization and tracking," in *Inclusive Radio Communications for 5G and Beyond*, C. Oestges and F. Quitin, Eds. Academic Press, 2021, pp. 253–293. [Online]. Available: https://www.sciencedirect.com/science/article/pii/B9780128205815000158

[9] M. Girolami, P. Barsocchi, F. Furfari, and M. Fabio, "A bluetooth 5.1 dataset based on angle of arrival and rss for indoor localization," 2023. [Online]. Available: https://dx.doi.org/10.5281/zenodo.7759557

[10] N. I. Piazzese, M. Perrone, and D. P. Pau, "Dataset for bluetooth 5.1 direction of arrival with non uniform rectangular arrays," *Data in Brief*, vol. 39, p. 107576, 2021. [Online]. Available: https://www.sciencedirect.com/science/article/pii/S2352340921008519

[11] G. Maus, H. Pörner, R. Schlenke, R. Ahrens, S. Janicke, P. Bolz, and E. Dürholt, "Bluetooth 5.1 angle of arrival based indoor localization," 2021. [Online]. Available: https://dx.doi.org/10.21227/2j4h-3w77

[12] G. Maus, H. Pörner, R. Ahrens, and D. Brückmann, "A phase normalization scheme for angle of arrival based bluetooth indoor localization," in *2022 IEEE 65th International Midwest Symposium on Circuits and Systems (MWSCAS)*, 2022.

[13] G. Maus, "Bluetooth direction finding for radar ranging," 2023. [Online]. Available: https://dx.doi.org/10.21227/zmqn-6y08

[14] G. Maus and S. Janicke, "Bluetooth direction finding for passive respiration monitoring," 2022. [Online]. Available: https://dx.doi.org/10.21227/wxj4-g666

[15] M. Girolami, P. Barsocchi, F. Furfari, D. La Rosa, and F. Mavilia, "Evaluation of angle of arrival in indoor environments with bluetooth 5.1 direction finding," in *2022 18th International Conference on Wireless and Mobile Computing, Networking and Communications (WiMob)*, 2022, pp. 284–289.

[16] F. Mavilia, P. Barsocchi, F. Furfari, D. La Rosa, and M. Girolami, "On the analysis of body orientation for indoor positioning with BLE 5.1 direction finding," in *2023 IEEE International Conference on Communications (ICC): IoT and Sensor Networks Symposium (IEEE ICC'23 - IoTSN Symposium)*, Rome, Italy, May 2023.

[17] F. Mavilia, P. Barsocchi, F. Furfari, and M. Girolami, "Evaluating the impact of anchors deployment for an aoa-based indoor localization system," in *2023 18th Wireless On-Demand Network Systems and Services Conference (WONS)*, 2023, pp. 20–23.

[18] G. Pau, F. Arena, Y. E. Gebremariam, and I. You, "Bluetooth 5.1: An analysis of direction finding capability for high-precision location services," *Sensors*, vol. 21, Art. no. 11, 2021. [Online]. Available: https://www.mdpi.com/1424-8220/21/11/3589

[19] P. Sambu and M. Won, "An experimental study on direction finding of bluetooth 5.1: Indoor vs outdoor," in *2022 IEEE Wireless Communications and Networking Conference (WCNC)*, 2022, pp. 1934–1939.

[20] F. Potortì and S. e. a. Park, "The ipin 2019 indoor localisation competition—description and results," *IEEE Access*, vol. 8, pp. 206 674–206 718, 2020.

[21] M. Barralet, X. Huang, and D. Sharma, "Effects of antenna polarization on rssi based location identification," in *2009 11th International Conference on Advanced Communication Technology*, vol. 1. IEEE, 2009, pp. 260–265.

[22] A. Kokkinis, L. Kanaris, A. Liotta, and S. Stavrou, "Rss indoor localization based on a single access point," *Sensors*, vol. 19, Art. no. 17, p. 3711, 2019.

[23] E. Teoman and T. Ovatman, "Trilateration in indoor positioning with an uncertain reference point," in *2019 IEEE 16th International Conference on Networking, Sensing and Control (ICNSC)*, 2019, pp. 397–402.

[24] N. O. Parchin, H. J. Basherlou, Y. I. A. Al-Yasir, A. Ullah, R. A. Abd-Alhameed, and J. M. Noras, "Frequency reconfigurable antenna array with compact end-fire radiators for 4g/5g mobile handsets," in *2019 IEEE 2nd 5G World Forum (5GWF)*, 2019, pp. 204–207.

[25] J. Dong, S. Wang, and J. Mo, "Design of a twelve-port mimo antenna system for multi-mode 4g/5g smartphone applications based on characteristic mode analysis," *IEEE Access*, vol. 8, pp. 90 751–90 759, 2020.

[26] P. Barsocchi, A. Calabrò, A. Crivello, S. Daoudagh, F. Furfari, M. Girolami, and E. Marchetti, "Covid-19 & privacy: Enhancing of indoor localization architectures towards effective social distancing," *Array*, vol. 9, Art. no. 100051, 2021. [Online]. Available: https://www.sciencedirect.com/science/article/pii/S2590005620300369

MICHELE GIROLAMI received his M.Sc. and Ph.D. in Computer Science from the University of Pisa respectively in 2007 and 2015. Currently he joins ISTI-CNR as Researcher with the Wireless Network Laboratory. He participates to several EU projects and as national research projects. His research interests are mainly focused on indoor localization, proximity detection, pervasive computing and Internet of Things. He also supports the organization of the IPIN competition and he has been serving with several roles for the organization of workshops and international conferences.

FRANCESCO FURFARI is senior researcher at the Information Science and Technology Institute (ISTI-CNR, Italy). His research interests include wireless sensor networks, mobile middleware, Internet of Things, and indoor localization. Furfari received his PhD in information engineering from the University of Pisa, Italy. Contact him at francesco.furfari@isti.cnr.it.

FABIO MAVILIA graduated in 2012 in Electronic Engineering at the University of Pisa. As a member of the Wireless Network Laboratory, he currently holds the position of Researcher at the Institute of Information Science and Technologies (ISTI), National Research Council of Italy (CNR). His research interests include Internet of Things and Cyber Physical Systems, with a particular focus on Ambient Intelligence. In particular, his work is focused on development of embedded platforms for wireless sensor networks and of algorithms for indoor activity recognition and for indoor localization, by using unobtrusive sensing devices based on radio frequency technologies.

PAOLO BARSOCCHI received the M.Sc. and Ph.D. degrees in information engineering from the University of Pisa, Italy, in 2003 and 2007, respectively. He is currently a Researcher with the Information Science and Technologies Institute, National Research Council, Pisa, Italy. He has coauthored more than one hundred articles published in international journals and conference proceedings. His research interests are mainly focused in the areas of the IoT, cyber-physical systems, indoor localization, and radio channel signal processing. He is also a member of numerous program committees and Editorial Board of international journals, and Program Chair and the Co-Chair of several conferences.